Analysis of microstructural images of dry and water-saturated compacted bentonite samples observed with X-ray micro CT

Satoshi Tomioka [a,*], Tamotsu Kozaki [a], Hidenori Takamatsu [a], Natsuko Noda [a], Shusuke Nisiyama [a], Naofumi Kozai [b], Satoru Suzuki [c,1], and Seichi Sato

[a] *Graduate School of Engineering, Hokkaido University, Kita 13 Nishi 8, Kita-ku, Sapporo, 060-8628 Japan*

[b] *Advanced Science Research Center, Japan Atomic Energy Agency (JAEA), Tokai, Ibaraki 319-1195, Japan*

[c] *Research Center for Deep Geological Environments, National Institute of Advanced Industrial Science and Technology, 1-1-1 Higashi, Tsukuba, Ibaraki, 305-8567, Japan*

Abstract

Compacted bentonite, of which the major clay mineral is montmorillonite, is a candidate buffer material for geological disposal of high-level radioactive waste. In this study, a microfocus X-ray computed tomography (micro-CT, X-ray microscope), which enables non-destructive, three-dimensional observation of the interior microstructure of a sample with high resolution (several microns), examined compacted montmorillonite samples under dry and water-saturated states. The images thus obtained were analyzed by a computer code developed for this study to obtain

the information on the size and shape of montmorillonite grains in the samples before and after the water saturation. From the results of the image analysis, it can be supposed that the outer montmorillonite sheets of grains swelled and formed a gel, whereas the inner montmorillonite sheets did not change significantly in the water-saturation process.

Key words: micro computed tomography, geological disposal, montmorillonite, compacted bentonite.

---

* Corresponding author: S. Tomioka; Graduate School of Engineering, Hokkaido University, Kita 13 Nishi 8, Kita-ku, Sapporo, 060-8628 Japan; E-mail: tom@qe.eng.hokudai.ac.jp, Tel.: +81-11-706-6656, Fax: +81-11-706-7128.

Email addresses: tom@qe.eng.hokudai.ac.jp (Satoshi Tomioka), kozaki@eng.hokudai.ac.jp (Tamotsu Kozaki).

[1] Present address: Science and Technology Department, Nuclear Waste Management Organization of Japan (NUMO), Mita NN building, 1-23, Shiba 4-chome, Minato-ku, Tokyo, 108-0014, Japan

1. Introduction

Compacted bentonite (or a mixture of bentonite and sand) is a candidate buffer material for geological disposal of high-level radioactive waste in Japan (JNC, 2000). The buffer material plays various important roles in the disposal system, e.g., to inhibit ground water flow and also to retard the migration of radionuclides in the region between the waste forms and the surrounding host rock. Since the properties of the buffer material are closely related to the microstructure of the bentonite, the study of the microstructure is a key issue for the safety assessment of geological disposal. Therefore, observations of the microstructure of compacted bentonite have been extensively performed using transmission electron microscopes (TEMs) and/or scanning electron microscopes (SEMs). Additionally, theoretical models for the microstructure of bentonite have been established (Pusch and Yong, 2006). However, further detailed knowledge of the microstructure of bentonite is still needed.

Three-dimensional imaging using X-ray computed tomography is a promising in-situ observation technique for geological materials (Carlson, 2006; Mooney, 2002; Nakashima, 2003). The advantage of this technique is that the interior of samples can be non-destructively examined. In addition, 3D imaging with high spatial resolution (several microns) has been realized with a microfocus X-ray computed tomography (micro-CT, X-ray microscope), as well as an X-ray CT using synchrotron radiation. Although there are several reports available for the X-ray CT observation of geological materials (DeVore et al., 2006; Nakashima et al., 2004; Van Geet et al., 2001; Van Geet et al., 2005), few attempts using the X-ray micro CT have been made to observe bentonite particles before and after water saturation (Kozaki et al., 2001; Liu et al.,

2003).

In this study, a newly developed X-ray micro CT having a high spatial resolution (about 0.8 μm under ideal conditions) was used to observe bentonite particles of compacted samples before and after water saturation. Computer code was newly developed for the analysis of micro-CT images to obtain information detailing the morphologic changes of bentonite grains before and after water saturation.

2. Experimental

The microfocus X-ray computed tomography used in this study is a SkyScan-1172 (Skyscan, Belgium). This system is comprised of an X-ray source (100 keV sealed microfocus tube with a spot size less than 5 μm), an air-cooled X-ray CCD camera having a resolution of 4000 x 2300 pixels, and a precision object manipulator. The detectable spatial resolution of this system is about 0.8 μm under ideal conditions.

Bentonite used in this study is Na-type montmorillonite, Kunipia-F, which is commercially available from Kunimine Industries, Japan. This sample contains montmorillonite ($>$ 95wt%) and minor components (Sato et al., 1992). The montmorillonite was purified into homoionic Na^+-type montmorillonite, ground by mortar and pestle, and then sieved to obtain a grain size of 75-150 μm, as described elsewhere (Kozaki et al., 1999). The purified montmorillonite samples were then compacted to a dry density of 1.0 Mg m^{-3} in glassy carbon tube (Tokai Carbon Co., LTD). Each tube had a 5-mm internal diameter and a 10-mm height. A negligibly small amount (*ca.* 1.3 vol.%) of glass spheres

(100-200 μm in diameter) was included in some montmorillonite samples as a reference. The montmorillonite samples which were fully saturated with water were prepared by contacting the compacted samples with distilled water through sintered stainless steel filters as illustrated in Fig. 1. After the water saturation period of more than two weeks, the cells were dismantled to expose the glassy carbon tubes. Both ends of each glassy carbon tube were sealed with a plastic plate held in place by adhesive to contain the water-saturated sample within the tube. The full water-saturations of the samples were confirmed in another experiment by weighing the samples before and after an oven-dry at 378 K.

The microstructures of the samples in the glassy carbon tubes were then observed with the micro-CT technique. The voltage of 50 kV was applied to the X-ray tube, and an aluminum filter (0.5 mm in thickness) was used in the observation. The samples were examined while being rotated 360 degrees in 0.1-degree steps. Data acquisition time was approximately 16 hours for each sample. The images obtained by 3D-reconstruction processes consist of 4000 x 4000 pixels with each pixel having an 8-bit attenuation value (i.e., signal intensity). The image spatial resolution was about 2 μm in this observation. The attenuation value of the X-ray corresponds to the image brightness at each pixel. The measurements and the 3D-reconstruction processes for all samples were carried out under identical conditions.

3. Analytical method using computer code

The two-dimensional micro-CT images were analyzed using a computer code developed for this study. The code employed three analytical steps; noise re-

duction, grain boundary analysis, and grain shape analysis. In the first step, a ring artifact reduction and image noise reduction were applied to the micro-CT images. In the second step, montmorillonite grains in the image were identified using a boundary determination algorithm. In the last step, the results were examined to determine several quantities associated with the montmorillonite particle grain shapes: the cross-sectional area, the length of the contour (perimeter), the length of the major, minor and mean axes, and the aspect ratio of each grain. Detailed procedures for each step are described below, together with the boundary determination algorithm and the parameters used for the calculations.

3.1. Noise reduction

The two-dimensional CT images contained 4000 x 4000 pixels, and each pixel was comprised of an 8-bit signal. In this study, a set of 256 pieces of two-dimensional CT images (horizontal plane of 400 x 400 pixels) was preconditioned to remove ring artifacts and random noise, and analyzed to obtain the grain shape information of the montmorillonite sample. Neither the glass beads nor any part of the glassy carbon sample holder was involved in the rectangular parallelepiped region of 400 x 400 x 256 pixels (*ca.* 800 x 800 x 500 μm).

The ring artifacts in the micro-CT images are observed as bright (or dark) concentric circles, of which the center of each is the same as the rotational center of the sample. Then, these artifacts were removed by a normalization in which the averaged intensities of pixels along every circle are assumed to be same. On the other hand, the random noise reduction procedure involved

two steps; spectrum analysis and filtering. The image spectrum contains the signals of grains in the lower spatial frequency region and widely distributed noise (Press et al., 1992). Assuming a model that contained the spectrum of superimposed signals with some Gaussian functions, white noise, and Gaussian shaped noise having wide spectral width; we determined the nature of each component of the spectrum using a nonlinear least-squares fit (Tomioka et al., 2007). The two types of noise (i.e., the white noise and the Gaussian shaped noise) were removed by a Gaussian spatial filter that had filtering parameters determined from the result of the nonlinear least-squares fit.

3.2. Grain boundary analysis

Grain boundaries of montmorillonite particles were discriminated by using a boundary determination algorithm included in the code. The scheme of the algorithm is shown in Fig. 2. In the algorithm, nodes having specific signal intensities were introduced in the image. The node was defined as the point at the center of each pixel, and the signal intensity was the same as that of the pixel. After a proper discrimination level of signal intensity for the grain boundary was determined, a point having the same value of signal intensity as the discrimination level was selected between two adjacent nodes. The position of this point was determined using linear interpolation. Segments of the grain boundary can be drawn with lines connecting adjacent points. The connecting lines were sequentially established in the direction of $\nabla f \times \boldsymbol{e}_z$, where f is signal intensity and $\boldsymbol{e}_z$ is the unit vector normal to the image plane (x-y plane). Since the direction ∇f is inward on the contour around the montmorillonite grains, the contour runs counter-clockwise. Using these steps, both closed and open

grain boundaries were obtained. However, only closed boundaries were utilized to define grains in this analysis; since an open grain boundary, which signifies that some portion of the grain was not in the image range, could lead to underestimated sizes and cross-sectional areas of grains.

3.3. Grain size analysis and shape analysis

By applying the above boundary determination algorithm to image data, the contours of all montmorillonite grains could be obtained except for grains with a portion of the grain not in the image. The circumference of a particular closed grain boundary, l, can be expressed by the following equation;

$$l = \sum_{j=0}^{N-1} \left| \boldsymbol{r}_j - \boldsymbol{r}_{j+1} \right|, \tag{1}$$

where N is the total number of points belonging to the contour, $\boldsymbol{r}_j$ is the location of the j-th point of a boundary line, and $\boldsymbol{r}_N$ is identical to $\boldsymbol{r}_0$.

On the other hand, the cross-sectional area of a grain can be calculated by the contour integral. According to Stokes' integral theorem, one relationship between a domain integral and a closed boundary integral can be given as follows;

$$\int \nabla \times \boldsymbol{A} \cdot \boldsymbol{n} \, dS = \oint \boldsymbol{A} \cdot \boldsymbol{t} \, dl, \tag{2}$$

where $\boldsymbol{A}$ is an arbitrary vector, $\boldsymbol{n}$ and $\boldsymbol{t}$ respectively denote a unit vector normal to a cross-sectional area dS and a unit vector tangential to a boundary dl.

When the closed boundary is on x-y plane, taking $\boldsymbol{n}$ to be $\boldsymbol{e}_z$, a vector $x\boldsymbol{e}_y$ can

be chosen as the arbitrary vector $\boldsymbol{A}$, which can satisfy the relation $\nabla \times \boldsymbol{A} = \boldsymbol{e}_z$, the area of closed grain boundary S can be given as follows;

$$S = \oint x\boldsymbol{e}_y \cdot \boldsymbol{t}\, dl = \oint x\, dy = \sum_{j=0}^{N-1} \frac{x_j + x_{j+1}}{2} \left(y_{j+1} - y_j\right). \tag{3}$$

In this equation, S of a montmorillonite grain is always positive because the signal intensities at any positions in the boundary surrounding the grain are larger than the discrimination level, and the contour integral path runs in the counter-clockwise direction. Conversely, the contours with a negative S value are considered to be internal holes in montmorillonite grains or vacancies surrounded by montmorillonite particles. In this study, therefore, the grain boundaries with a negative S value were omitted from the analysis.

The major axis of a montmorillonite grain, d_L, is defined as the longest distance between two points among all possible pairs of points on a grain boundary as follows;

$$d_L = \max_{i,j} \left|\boldsymbol{r}_i - \boldsymbol{r}_j\right|, \qquad (i, j \in 0, \cdots, N-1). \tag{4}$$

By assuming the montmorillonite grain to be elliptical, the area, S, can be expressed as follows;

$$S = \pi \frac{d_L}{2} \frac{d_S}{2}, \tag{5}$$

where d_S is the minor axis of the montmorillonite grain. Consequently, the minor axis, d_S, can be given by the following equation;

$$d_S = \frac{4S}{\pi d_L}. \tag{6}$$

In addition, the mean diameter of grains, d_m, can be given as the geometrical average by the following equation;

$$d_m = \sqrt{d_L d_S} = 2\sqrt{\frac{S}{\pi}}. \tag{7}$$

The aspect ratio of grains, α, can be defined by the following equation;

$$\alpha = \frac{d_S}{d_L} = \frac{4S}{\pi d_L^2}. \tag{8}$$

4. Results and discussion

4.1. Microstructure of dry-state compacted montmorillonite

The brightness of a CT-image corresponds to the attenuation of the X-rays, which depends on the atomic numbers of the elements and their densities in a sample. A typical horizontal-plane, two-dimensional, micro-CT image of a dry montmorillonite sample at a dry density of 1.0 Mg m^{-3} is shown in Fig. 3. In this figure, montmorillonite particles can be clearly identified as ellipse-shaped dapples (gray spots) inside the big dark gray ring, which is the glassy carbon sample holder. On the other hand, the glass spheres introduced as a reference can be identified as reasonably large, definitely circular dapples (bright spots) anywhere in the image. This suggests that the CT apparatus used in this study can precisely reproduce distinct images of masses in a sample with at least a resolution of several microns.

Figure 4 shows the frequency distribution of pixels as a function of signal intensity that was obtained for a dry montmorillonite sample. The frequency

varied continuously but has a high peak at a signal intensity of 70 and a lower peak at a signal intensity of 140. It seems that pixels at the signal intensity of 70 and 140 correspond to air-filled void spaces and montmorillonite particles, respectively. In addition, the continuous distribution suggests that there are a certain number of pixels in which air and montmorillonite coexist at various ratios. These result in pixels with grayish color in the Fig. 3 image. The montmorillonite grain boundaries, therefore, should be evaluated with an appropriate threshold value (discrimination level). In this study, the discrimination level was determined by assuming that the numerical ratio of bright pixels to the whole pixels was identical to the theoretical volumetric fraction of the solid (montmorillonite), η, which can be given by the following equation;

$$\eta = \frac{V^c}{V^{all}} = \frac{\rho - \rho_a}{\rho_c - \rho_a}, \tag{9}$$

where V^c is the volume of montmorillonite, V^{all} is the total volume of the sample, ρ_c is the partial density of montmorillonite (2.88 Mg m^{-3}), ρ_a is the absolute density of air ($\sim$0 Mg m^{-3}), and ρ is the dry density of montmorillonite (i.e., the packing density in dry condition; 1.0 Mg m^{-3}). In this case, the value of η becomes 0.347. For the dry montmorillonite sample, the threshold value to discriminate grain boundaries can be determined to be 103.2, which is in accordance with the signal intensity at the accumulated frequency of 0.653 ($= 1 - 0.347$) in Fig. 4.

Figure 5 shows grain boundaries determined by the computer code with a discrimination level of 103.2 for the image of the dry montmorillonite sample at the dry density of 1.0 Mg m^{-3}, together with images before and after the noise reduction. The dapples drawn by solid lines are montmorillonite particles recognized by the code, whereas dapples drawn by dotted lines are closed void

spaces surrounded with montmorillonite or portions of montmorillonite particles that were not in the image range. The total number of montmorillonite grains identified with the computer code was approximately 24,000.

The distribution of the mean diameter of the boundaries of grains analyzed with the algorithm discussed in the section 3.3 is shown in Fig. 6. The grains, which had been sieved to 75-150 μm in the sample preparation process, have wide peaks in the mean diameters around 100 μm. Consequently, it follows that the images obtained by micro-CT examinations represent the interior microstructures of the dry montmorillonite. Further, the combination of micro-CT and the code enables us to evaluate the microstructures of the dry compacted montmorillonite samples with high resolution.

4.2. Microstructure of water-saturated compacted montmorillonite

In the case of water-saturated montmorillonite samples, water in the sample may attenuate both the intensity and the energy of the X-rays, resulting in unclear images with artifacts. In addition, the homogenization of the montmorillonite caused by the water saturation may make it difficult to determine a proper discrimination level for grain boundaries during the image analysis.

A typical horizontal plane, two-dimensional, micro-CT image of a water-saturated montmorillonite sample at a dry density of 1.0 Mg m^{-3} is shown in Fig. 7. Montmorillonite particles are unable to be clearly recognized in the image, although glass spheres still can be identified as circular dapples. Therefore, water saturation can homogenize the montmorillonite sample, at least in the scale of this spatial resolution (about 2 μm). Figure 8 is a plot of the fre-

quency distribution of pixels in the image of water-saturated montmorillonite as a function of signal intensity. This also suggests that the montmorillonite sample becomes almost homogeneous following water saturation, since there is only one sharp peak in the figure. However, small patches with slightly higher brightness seem to be present in the image of the water-saturated montmorillonite shown in Fig. 7. Therefore, the same analysis as for the dry sample was applied to the water-saturated sample in this study.

The spectral analysis detected significant signals in low spatial frequency range which was not noise. This suggests the presence of objects in the image. The discrimination level of 141.9 was used for the image of the water-saturated montmorillonite sample, as shown in Fig. 8. This discrimination level could produce overestimated values of grain sizes, since the level was determined by assuming the numerical ratio of bright pixels to the whole pixels was identical to the theoretical volumetric fraction of the solid, i.e. η; a fraction of gel phase was needed to be recognized as solid phase in order to attain the same numerical ratio as the theoretical volumetric fraction. Figure 9 shows an example of grain boundaries of the water-saturated montmorillonite determined with the computer code using the discrimination level, with the images before and after the noise reduction. The total number of grains identified with the computer code was about 12,000, which is almost half of that in the dry condition. This decrease in the total number of grains can be attributed to the increase in the open grain boundary, which signifies that some portion of the grain was not in the image, as mentioned above. As compared with Fig. 5(c), the grains in the water-saturated sample (Fig. 9(c)) seem to be smaller than those in the dry sample (Fig. 5(c)). To compare them quantitatively, the mean diameter distribution of the water-saturated montmorillonite grains analyzed

with the computer code together with that of the dry sample is shown in Fig. 6. Realizing that the grain sizes could be overestimated in the image of the water-saturated sample, it is obvious that the grain sizes decreased with the water saturation.

On the other hand, in the X-ray diffraction study of water-saturated, compacted montmorillonite, the diffraction peak of 1.88 nm, which corresponds to the three-water-layer hydrate state of the montmorillonite interlayer, was reported to emerge at the dry density of 1.0 Mg m^{-3}. However, there was no peak below this dry density (Kozaki et al., 1998). This fact suggests that the montmorillonite at this dry density still has dense fragments (indicated by the diffraction peak) even after the water saturation. It is very likely that the dense fragments correspond to the grains that were identified in Fig. 9 with the computer code for the water-saturated montmorillonite.

Figure 10 indicates the distributions of the grain aspect ratio (i.e., the ratio of the minor axis to the major axis) before and after water saturation. No significant change in grain aspect ratio was found in the images before and after water saturation. Then, except the region of the open grain boundaries, it can be supposed that the outer montmorillonite sheets of grains swelled and formed a gel, whereas the inner sheets did not change significantly in the water-saturation process, as illustrated in Fig. 11. The gel that formed could occupy the vacancies between grains. This kind of model for water-saturation of montmorillonite had been proposed elsewhere (Pusch et al., 2006). However, in the analysis of the micro-CT image with the computer code in this study, some portions of gel with slightly higher density could be recognized as a part of or the whole of montmorillonite particles as illustrated with dark gray color in Fig. 11, due to the overestimation for the solid phase in the grain boundary

determination algorithm. This is a possible reason for the small changes in the grain aspect ratios before and after the water-saturation.

5. Conclusion

The nondestructive, three-dimensional images of the internal microstructures of compacted montmorillonite samples in dry and water-saturated states were obtained with the micro-CT, and analyzed with the computer code developed in this study. The code could determine grain boundaries of montmorillonite in the images by using appropriate discrimination levels, and provide information on size and shape of montmorillonite grains, such as the mean diameter and the aspect ratio of montmorillonite grains. From the results of this analysis, it is supposed that the outer montmorillonite sheets of grains swelled and formed a gel, whereas the inner sheets did not change significantly in the water-saturation process.

Acknowledgements

The authors express their appreciation to Mr. T. Ohyagi and Ms. Y. Mizuguchi, TOYO Corporation, for providing us with the opportunity to use the micro-CT apparatus and for their technical suggestions regarding these experiments. The authors wish to thank Professors M. Nakano and R. Pusch for their valuable suggestions. Financial support was provided by the Ministry of Education, Culture, Sports, Science and Technology (MEXT), Japan (a Grant-in-Aid for Scientific Research (C), No. 17560049), the Japan Atomic Energy Agency (JAEA), and the Radioactive Waste Management Funding and Research Cen-

ter (RWMC).

References

Carlson, W.D., 2006. Three-dimensional imaging of earth and planetary materials. Earth and Planetary Science Letters 249, 133-147.

DeVore, M.L., Kenrick, P., Pigg, K.B., Ketcham, R.A., 2006. Utility of high resolution x-ray computed tomography (HRXCT) for paleobotanical studies: An example using London Clay fruits and seeds. American Journal of Botany 93, 1848-1851.

Japan Nuclear Cycle Development Institute (JNC), 2000. H12: project to establish the scientific and technical basis for HLW disposal in Japan, supporting report 3 safety assessment of the geological disposal system. JNC Technical Report, JNC TN 1400 2000-04.

Kozaki, T., Fujishima, A., Sato, S., Ohashi, H., 1998. Self-diffusion of sodium ions in compacted sodium montmorillonite. Nuclear Technology 121, 63-69.

Kozaki, T., Sato, Y., Nakajima, M., Kato, H., Sato, S., Ohashi, H., 1999. Effect of particle size on the diffusion behavior of some radionuclides in compacted bentonite. Journal of Nuclear Materials 270, 265-272.

Kozaki, T., Suzuki, S., Kozai, N., Sato, S., Ohashi, H., 2001. Observation of microstructures of compacted bentonite by microfocus X-ray computerized tomography (micro-CT). Journal of Nuclear Science and Technology 38, 697-699.

Liu, J., Kozaki, T., Horiuchi, Y., Sato, S., 2003. Microstructure of montmorillonite/silica sand mixture and its effects on the diffusion of strontium ions. Applied Clay Science 23, 89-95.

Mooney, S.J., 2002. Three-dimensional visualization and quantification of soil

macroporosity and water flow patterns using computed tomography. Soil Use and Management 18, 142-151.

Nakashima, Y., 2003. Diffusivity measurement of heavy ions in Wyoming montmorillonite gels by X-ray computed tomography. Journal of Contaminant Hydrology 61, 147-156.

Nakashima, Y., Nakano, T., Nakamura, K., Uesugi, K., Tsuchiyama, A., Ikeda, S., 2004. Three-dimensional diffusion of non-sorbing species in porous sandstone: computer simulation based on X-ray microtomography using synchrotron radiation. Journal of Contaminant Hydrology 74, 253-264.

Press, W.H., Teukolsky, S.A., Vettering, W.T., Flannery, B.P., 1992. Fourier and Spectral Applications. in: Numerical Recipes in Fortran 77: the art of scientific computing, Second ed. Press Syndicate of the University of Cambridge, New York & Melbourne.

Pusch, R., Yong, R.N., 2006. Microstructure of smectite clays and engineering performance. Taylor & Francis, London & New York.

Sato, H., Ashida, T., Kohara, Y., Yui, M., Sasaki, N., 1992. Effect of dry density on diffusion of some radionuclides in compacted sodium bentonite. Journal of Nuclear Science and Technology 29, 873-882.

Tomioka, S., Nisiyama, S., Enoto, T., 2007. Nonlinear least square regression by adaptive domain method with multiple genetic algorithms. IEEE transactions on Evolutionary Computation 11, 1-16.

Van Geet, M., Swennen, R., David, P., 2001. Quantitative coal characterisation by means of microfocus X-ray computer tomography, colour image analysis and back-scattered scanning electron microscopy. International Journal of Coal Geology 46, 11-25.

Van Geet, M., Volckaert, G., Roels, S., 2005. The use of microfocus X-ray computed tomography in characterising the hydration of a clay pellet/powder

mixture. Applied Clay Science 29, 73-87.

List of Figures

Fig. 7 A typical horizontal plane, two-dimensional, micro-CT image of a water-saturated montmorillonite sample (grain size: 75-100 μm; dry density: 1.0 Mg m^{-3}). This sample contained glass spheres having diameter of 100-200 μm.

Fig. 8 Signal intensity distribution of pixels in all images included in a set of CT data of a water-saturated montmorillonite sample (grain size: 75-100 μm; dry density: 1.0 Mg m^{-3}); thin and thick lines represent frequency and accumulated frequency, respectively.

Fig. 9 Image processing of a CT image of a water-saturated montmorillonite sample: (a) original image, (b) preconditioned image by using the ring artifact reduction technique and Gaussian filtering in which image contrast is enhanced to four times that of the original image, (c) extracted boundaries from the preconditioned image by grain boundary determination algorithm.

Fig. 10 Aspect ratio distribution montmorillonite grains before and after water-saturation. Lines with and without square symbols represent accumulated area fraction and area fraction, respectively.

Fig. 11 Schematic of the structures of montmorillonite : (a) in dry state, (b) in water-saturated state.

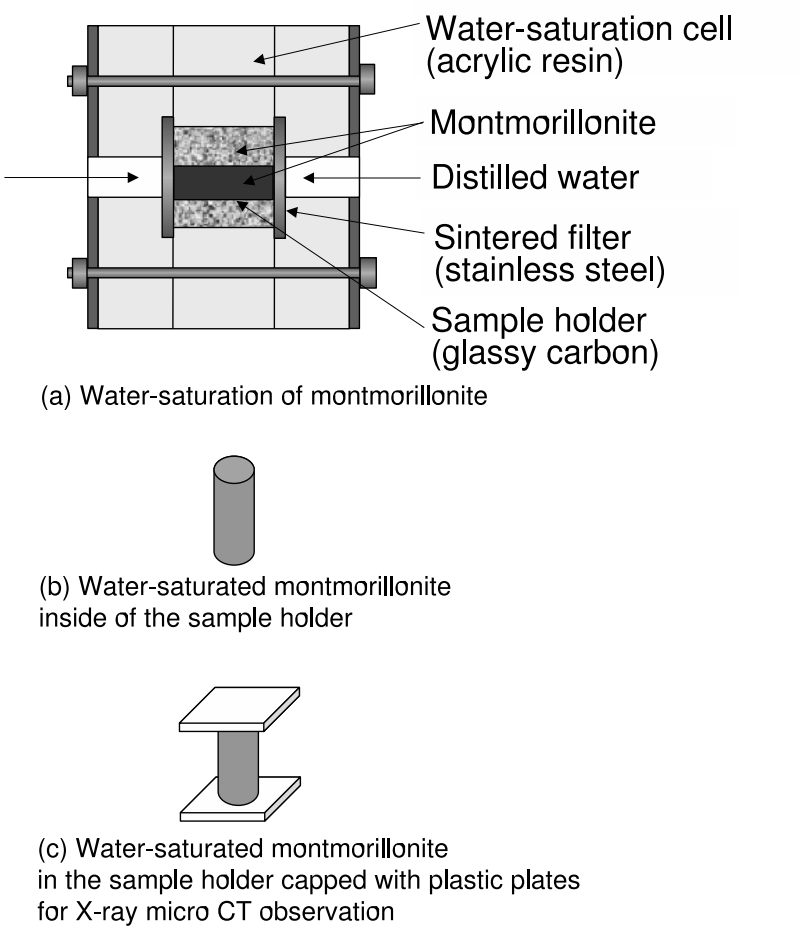

Fig. 1. Preparation of the watar-saturated sample.

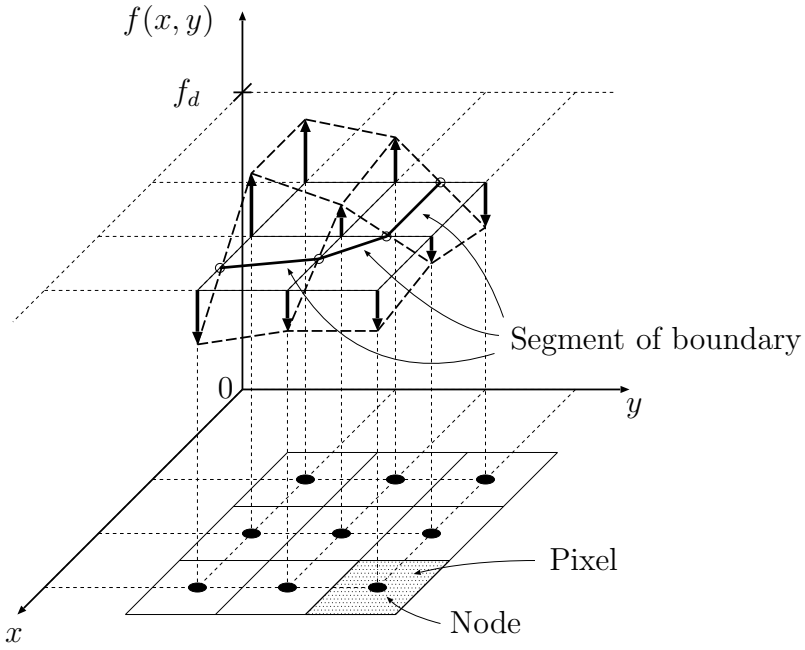

Fig. 2. Schematic of boundary determination algorithm.

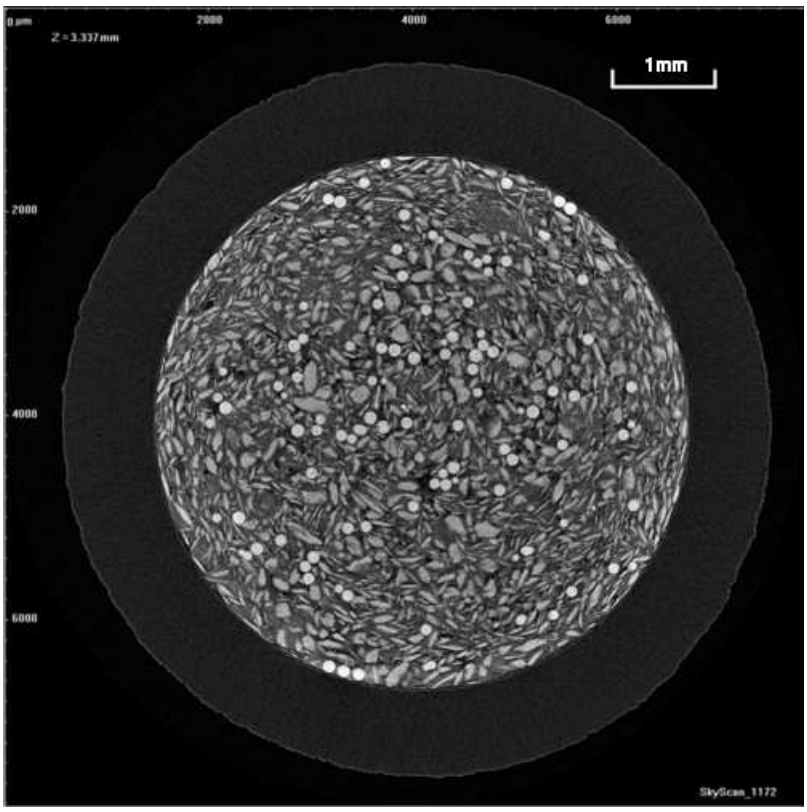

Fig. 3. A typical horizontal plane, two-dimensional, micro-CT image of a dry montmorillonite sample (grain size: 75-100 μm; dry density: 1.0 Mg m^{-3}). This sample contained glass spheres having diameters of 100-200 μm.

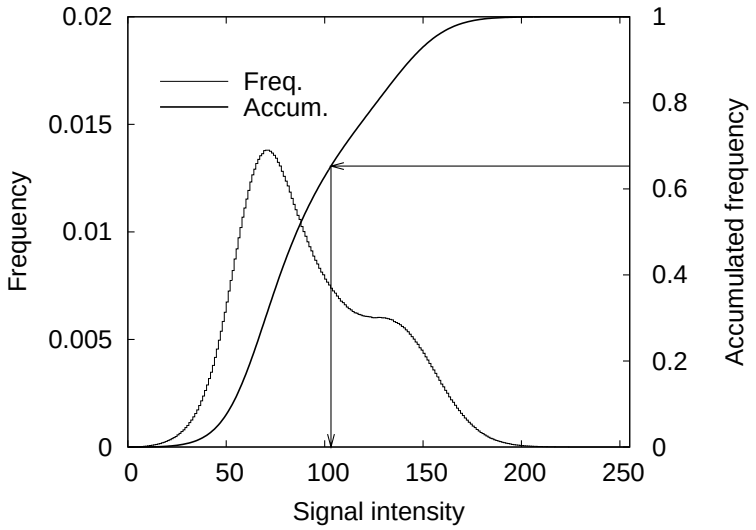

Fig. 4. Signal intensity distribution of pixels in all images included in a set of CT data of a dry montmorillonite sample (grain size: 75-100 μm; dry density: 1.0 Mg m^{-3}); thin and thick lines represent frequency and accumulated frequency, respectively.

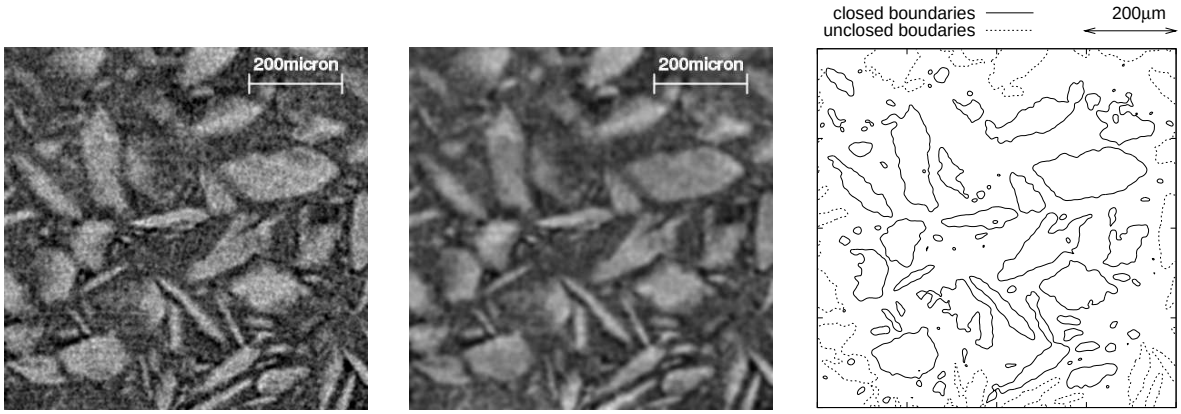

Fig. 5. Image processing of a CT image of a dry montmorillonite sample: (a) original image, (b) preconditioned image by using the ring artifact reduction technique and Gaussian filtering, (c) extracted boundaries from the preconditioned image by using the grain boundary determination algorithm.

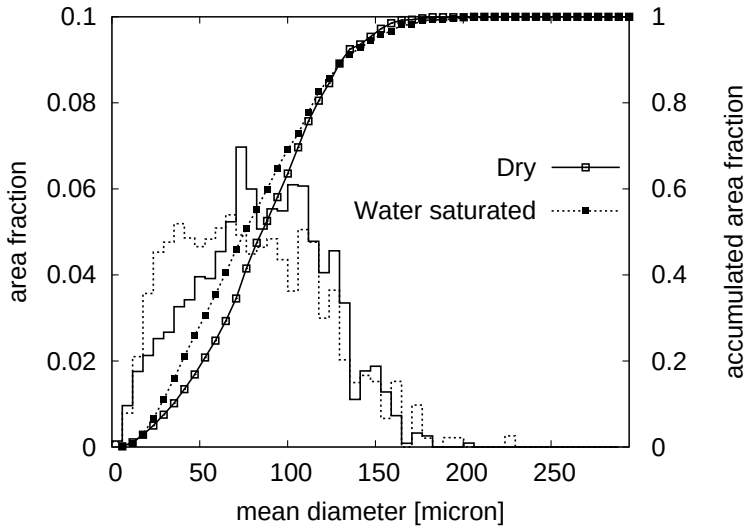

Fig. 6. Mean diameter distribution of montmorillonite grains before and after water saturation. Lines with and without square symbols represent accumulated area fraction and area fraction, respectively.

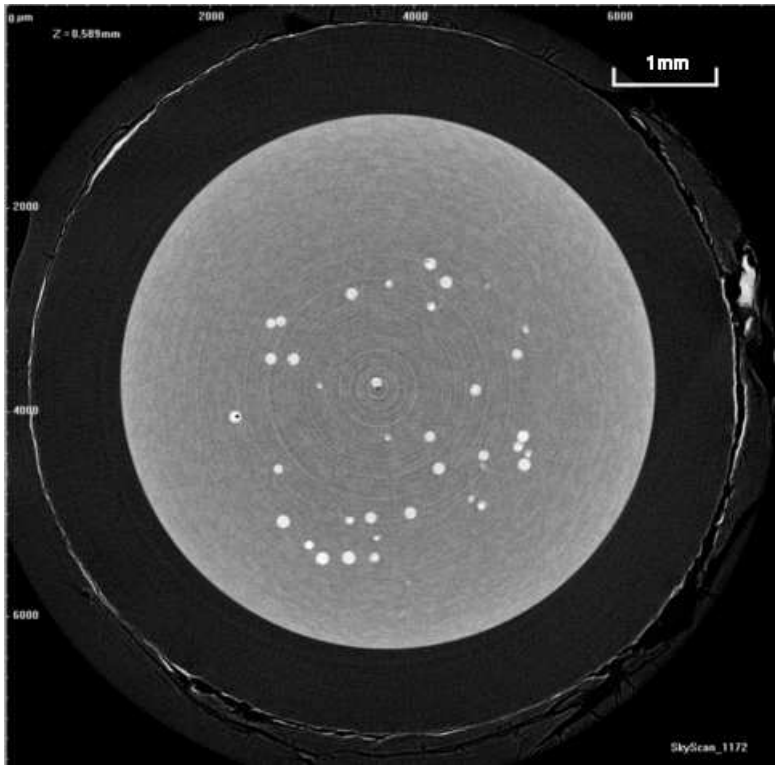

Fig. 7. A typical horizontal plane, two-dimensional, micro-CT image of a water-saturated montmorillonite sample (grain size: 75-100 μm; dry density: 1.0 Mg m^{-3}). This sample contained glass spheres having diameter of 100-200 μm.

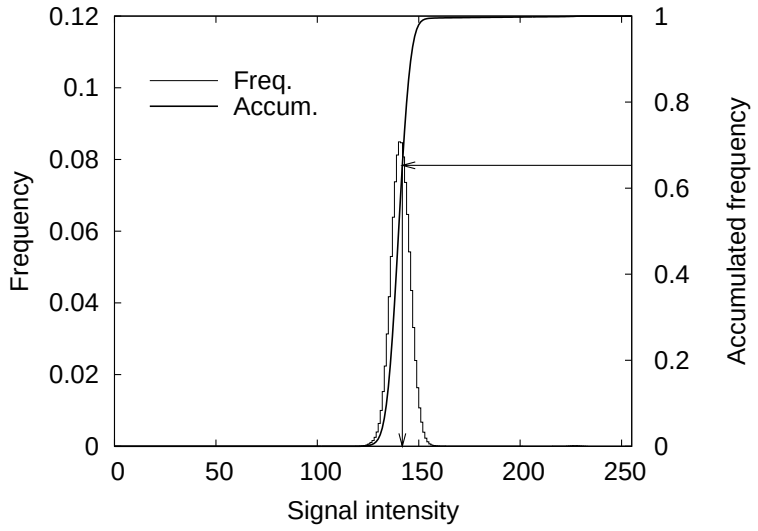

Fig. 8. Signal intensity distribution of pixels in all images included in a set of CT data of a water-saturated montmorillonite sample (grain size: 75-100 μm; dry density: 1.0 Mg m^{-3}); thin and thick lines represent frequency and accumulated frequency, respectively.

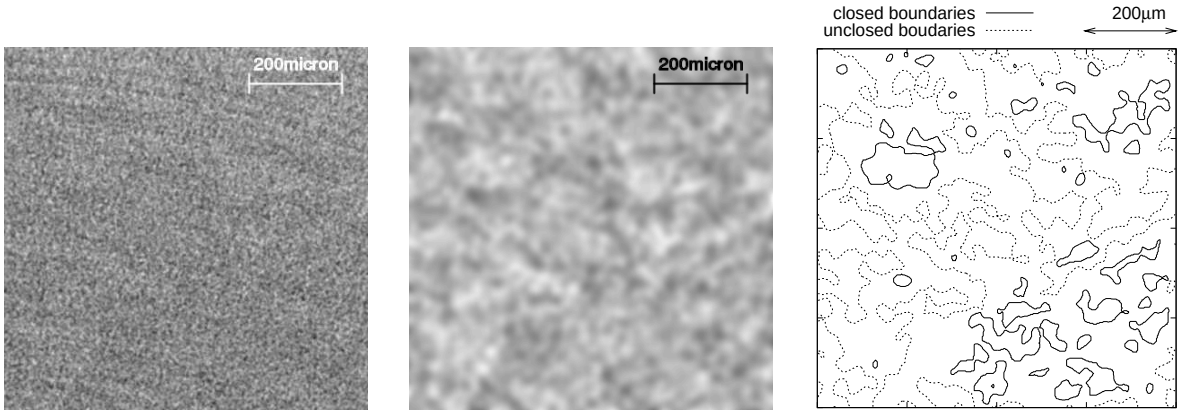

Fig. 9. Image processing of a CT image of a water-saturated montmorillonite sample: (a) original image, (b) preconditioned image by using the ring artifact reduction technique and Gaussian filtering in which image contrast is enhanced to four times that of the original image, (c) extracted boundaries from the preconditioned image by grain boundary determination algorithm.

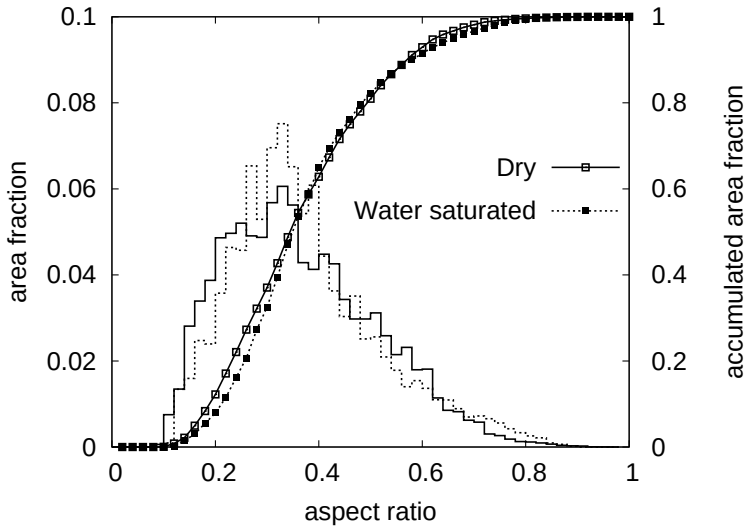

Fig. 10. Aspect ratio distribution montmorillonite grains before and after water-saturation. Lines with and without square symbols represent accumulated area fraction and area fraction, respectively.

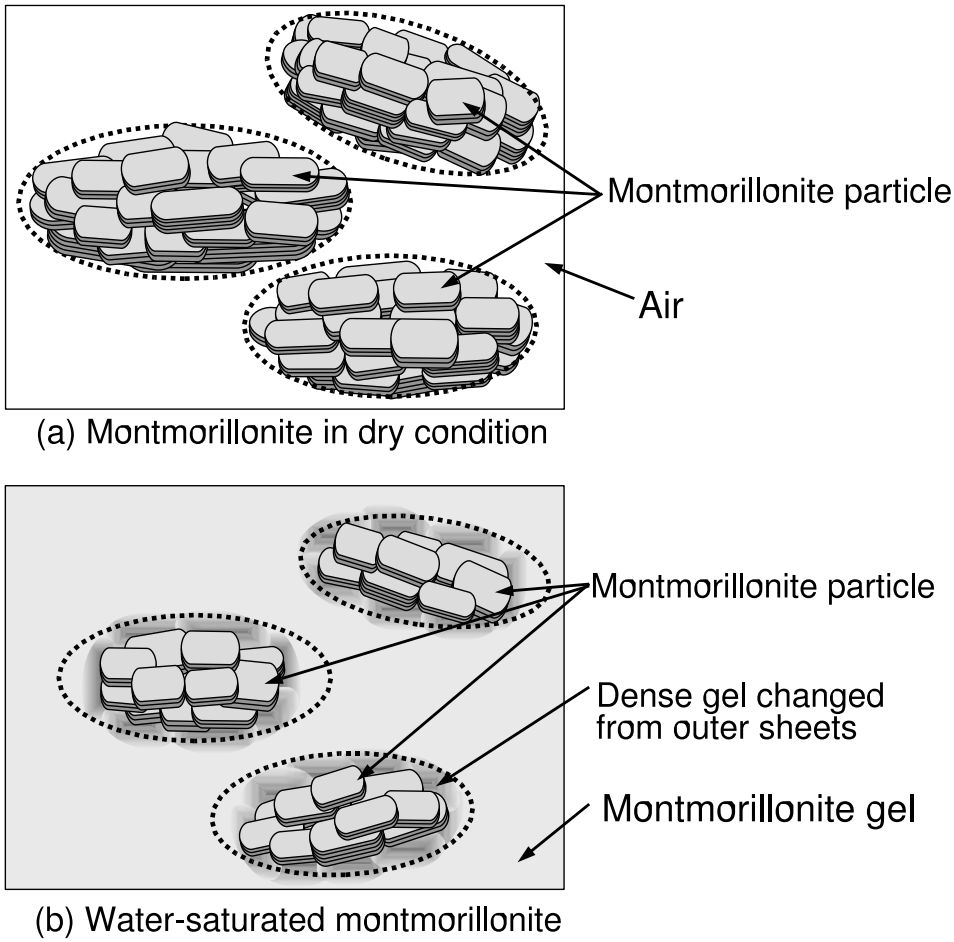

Fig. 11. Schematic of the structures of montmorillonite : (a) in dry state, (b) in water-saturated state.